Fluence correction factor for graphite calorimetry in a clinical high-energy carbon-ion beam

Fluence correction factor for graphite calorimetry in a clinical high-energy carbon-ion beam

A Lourenço[1,2], R Thomas[2], M Homer[2], H Bouchard[3], S Rossomme[4], J Renaud[5], T Kanai[6], G Royle[1], H Palmans[2,7]

1 - Department of Medical Physics and Biomedical Engineering, University College London, London WC1E 6BT, United Kingdom
2 - Division of Acoustics and Ionising Radiation, National Physical Laboratory, Teddington TW11 0LW, United Kingdom
3 - Departement de Physique, Universite de Montreal, 2900 Boulevard Edouard-Montpetit, Montreal, Canada
4 - Center of Molecular Imaging, Radiotherapy and Oncology, Insitut de recherche expérimentale et clinique, Université catholique de Louvain, Brussels, Belgium
5 - Medical Physics Unit, McGill University, Montréal, Quebec H3G 1A4, Canada
6 - Gunma University Heavy Ion Medical Center, Gunma University, Showa 3-39-22, Maebashi, Gunma 371-8511, Japan
7- Medical Physics Group, EBG MedAustron GmbH, A-2700 Wiener Neustadt, Austria

am.lourenco@ucl.ac.uk

Abstract

The aim of this work is to develop and adapt a formalism to determine absorbed dose to water from graphite calorimetry measurements in carbon-ion beams. Fluence correction factors, k_{fl}, needed when using a graphite calorimeter to derive dose to water, were determined in a clinical high-energy carbon-ion beam. Measurements were performed in a 290 MeV/n carbon-ion beam with a field size of 11 x 11 cm^2, without modulation. In order to sample the beam, a plane-parallel Roos ionization chamber was chosen for its small collecting volume in comparison with the field size. Experimental information on fluence corrections was obtained from depth-dose measurements in water. This procedure was repeated with graphite plates in front of the water phantom. Fluence corrections were also obtained with Monte Carlo simulations through the implementation of three methods based on (i) the fluence distributions differential in energy, (ii) a ratio of calculated doses in water and graphite at equivalent depths and (iii) simulations of the experimental setup. The k_{fl} term increased in depth from 1.00 at the entrance toward 1.02 at a depth near the Bragg peak, and the average difference between experimental and numerical simulations was about 0.13%. Compared to proton beams, there was no reduction of the k_{fl} due to alpha particles because the secondary particle spectrum is dominated by projectile fragmentation. By developing a practical dose conversion technique, this work contributes to improving the determination of absolute dose to water from graphite calorimetry in carbon-ion beams.

1. Introduction

The quantity of interest in radiation therapy dosimetry is absorbed dose to water. The determination of this quantity must be accurate, reproducible and traceable in order to assure tumour control and mitigate normal tissue complications. Calorimeters determine absorbed dose by measuring the temperature rise in the medium as a result of radiation. These devices are the recommended primary standards to measure absorbed dose in x-ray and electron beams and numerous efforts have been reported on the establishment of calorimeters as primary standard instruments for light-ion beams as well [Palmans *et al.*, 2004 and 2007, Brede *et al.*, 2006, Sakama *et al.*, 2009, Medin, 2010, Sarfehnia *et al.*, 2010]. Graphite calorimeters have been developed due to their advantageous higher sensitivity and good tissue-equivalence [AAPM, 1986, Vynckier *et al.* 1991 and 1994, ICRU, 1998]. However, a conversion procedure is required to determine absorbed dose to water. The latter is the disadvantage of graphite calorimetry because it increases the total uncertainty of absorbed dose to water. The conversion requires (i) the stopping-power ratio between water and graphite and (ii) the fluence correction factor, k_{fl}, that corrects for the difference between the fluence distributions at equivalent depths in the two materials [Lühr *et al.*, 2011, Palmans *et al.*, 2013, Rossomme *et al.*, 2013]. The necessity of k_{fl} stems from the differences between the non-elastic nuclear interactions cross sections in oxygen and other nuclei. These interactions attenuate the primary

beam fluence and the rate of production of secondary particles will be different, depending on the composition of the medium. In addition to graphite calorimetry, fluence corrections are also relevant when water-equivalent plastics are used in dosimetry [Palmans *et al.*, 2002, Schneider *et al.*, 2002, Lühr *et al.*, 2011, Lourenço *et al.*, 2016a] and in the comparison of dose calculations performed with Monte Carlo codes, which calculate dose to tissue, and treatment planning systems, which typically calculate dose to water [Paganetti, 2009].

Several studies were performed to determine k_{fl} for graphite calorimetry in light-ion beams. Lühr *et al.* (2011) determined fluence correction factors and stopping-power ratios for graphite, bone and PMMA using Monte Carlo methods in clinical light-ion beams using the SHIELD-HIT code. Results from graphite showed that fluence corrections were small for low-energy beams, with a variation in depth below 1%, while for high-energy beams the correction was larger, with a variation in depth of 2% for carbon-ion beams and 5% for proton beams. Overall, the authors reported that fluence corrections for higher-energy beams could be significant and needed to be investigated. Rossomme *et al.* (2013) performed an experimental and numerical comparison of k_{fl} values between water and graphite for an 80 MeV/n carbon-ion beam, where experimental information was obtained from ionization chamber measurements in water and graphite. In their work, the ratio of ionization chamber perturbation correction factors between water and graphite was assumed negligible although this ratio is not well known. The authors reported disagreements between fluence correction factors calculated numerically and experimentally which suggested that the ratio of ionization chamber perturbation correction factors between graphite and water is not negligible and it should be considered in the analysis.

In this work, k_{fl} was determined experimentally and compared with Monte Carlo simulations for graphite calorimetry, extending previous work [Rossomme *et al.*, 2013] by adding an alternative experimental setup that is independent of ionization chamber perturbation correction factors as well as by studying this topic in a broad high-energy carbon-ion beam.

2. Theory

2.1. Calculation methods for the fluence correction factor, k_{fl}

2.2.1 Monte Carlo approach. Using Monte Carlo methods, fluence correction factors were calculated based on the fluence distributions differential in energy, $\Phi_E(E)$, in water (w) and graphite (g) at equivalent depths [Palmans *et al.*, 2013]:

$$k^{\mathrm{MC}}_{\mathrm{fl,fluence}}(z_{\mathrm{w-eq}}) = \frac{\sum_i \left[\int_0^{E_{\max,i}} \Phi^{(1)}_{E,\mathrm{w},i}(E).\left(\frac{S_i(E)}{\rho}\right)_{\mathrm{w}}.\mathrm{d}E\right]}{\sum_i \left[\int_0^{E_{\max,i}} \Phi^{(2)}_{E,\mathrm{g},i}(E).\left(\frac{S_i(E)}{\rho}\right)_{\mathrm{w}}.\mathrm{d}E\right]} \qquad (1)$$

where i is the charged particle type and S/ρ is the mass stopping power. The numbers in superscript (i.e. 1 and 2) identify the setups used. In setup #1, quantities were scored in a homogenous phantom of water and in setup #2 quantities were scored in a homogenous phantom of graphite (figure 1). An alternative method was also used to compute fluence correction factors based on a ratio of calculated doses:

$$k^{\mathrm{MC}}_{\mathrm{fl,dose}}(z_{\mathrm{w-eq}}) = \frac{D^{(1)}_{\mathrm{w}}\left(z_{\mathrm{w-eq}}\right)}{D^{(2)}_{\mathrm{g}}\left(z^{(2)}_{\mathrm{g}}\right).s^{\mathrm{BG}}_{\mathrm{w,g}}(\Phi^{(2)}_{\mathrm{g}})} \qquad (2)$$

where $D^{(1)}_{\mathrm{w}}$ and $D^{(2)}_{\mathrm{g}}$ are the doses in water and graphite, respectively, and $s^{\mathrm{BG}}_{\mathrm{w,g}}$ is the water-to-graphite Bragg-Gray stopping-power ratio. Depths in setups #1, $z^{(1)}_{\mathrm{w}}$, and in #2, $z^{(2)}_{\mathrm{g}}$, are related by the ratio of ranges in each setup. A detailed description of equations (1) and (2) can be found in the work of Palmans *et al.* (2013).

2.2.2 Graphite phantom approach. Similar to Palmans *et al.* (2013), Rossomme *et al.* (2013) calculated fluence correction factors between water and graphite using setups #1 and #2. Experimental information on fluence corrections was obtained from ionization chamber measurements employing the following formalism. By application of the Spencer-Attix cavity theory, absorbed dose to medium $D^{(n)}_m$ at a depth of measurement $z^{(n)}_m$, is related to the ionization chamber reading $M^{(n)}$ by:

$$D^{(n)}_m(z^{(n)}_m) = M^{(n)}(z^{(n)}_m).\frac{W^{(n)}_{\mathrm{air}}/e}{m_{\mathrm{air}}}.s^{\mathrm{SA}}_{m,\mathrm{air}}(\Phi^{(n)}_m).p^{(n)}_m(z^{(n)}_m) \qquad (3)$$

where $W_{\text{air}}^{(n)}$ is the mean energy required to produce an ion pair in air, e is the charge of the electron, m_{air} is the mass of air in the chamber, $s_{\text{m,air}}^{\text{SA}}$ is the medium-to-air Spencer-Attix stopping-power ratio for the fluence in medium m, and $p_m^{(n)}$ the perturbation correction factor for the chamber in medium m. Note that Spencer-Attix stopping powers consider the production of secondary electrons (or delta-rays) that have enough energy to travel away from the point where they were generated before their energy is deposited. An energy threshold is defined above which secondary electrons are transported and their energy is deposited away from the initial site of interaction and restricted stopping powers are used to account for such energy exchanges. On the other hand, Bragg-Gray stopping powers consider that secondary electrons deposit their energy locally. The energy threshold is set to infinity and unrestricted stopping powers are used.

Using equation (3), the ratio of ionization chamber readings between water and graphite at equivalent depths is given by:

$$\frac{M^{(1)}(z_{\text{w-eq}})}{M^{(2)}(z_{\text{g}}^{(2)})} = \frac{D_{\text{w}}^{(1)}(z_{\text{w-eq}})}{D_{\text{g}}^{(2)}(z_{\text{g}}^{(2)}).\frac{W_{\text{air}}^{(1)}/e}{W_{\text{air}}^{(2)}/e}.\frac{s_{\text{w,air}}^{\text{SA}}(\Phi_{\text{w}}^{(1)})}{s_{\text{g,air}}^{\text{SA}}(\Phi_{\text{g}}^{(2)})}.\frac{p_{\text{w}}^{(1)}(z_{\text{w-eq}})}{p_{\text{g}}^{(2)}(z_{\text{g}}^{(2)})}} \quad (4)$$

By multiplying and dividing the denominator on the right hand side by $s_{\text{w,air}}^{\text{BG}}(\Phi_{\text{w}}^{(1)}).s_{\text{g,air}}^{\text{BG}}(\Phi_{\text{g}}^{(2)}).s_{\text{w,air}}^{\text{BG}}(\Phi_{\text{g}}^{(2)})$, one obtains

$$\frac{M^{(1)}(z_{\text{w-eq}})}{M^{(2)}(z_{\text{g}}^{(2)})} = \frac{D_{\text{w}}^{(1)}(z_{\text{w-eq}})}{D_{\text{g}}^{(2)}(z_{\text{g}}^{(2)}).s_{\text{w,g}}^{\text{BG}}(\Phi_{\text{g}}^{(2)})}.\frac{W_{\text{air}}^{(2)}/e}{W_{\text{air}}^{(1)}/e}.\frac{\frac{s_{\text{g,air}}^{\text{SA}}(\Phi_{\text{g}}^{(2)})}{s_{\text{g,air}}^{\text{BG}}(\Phi_{\text{g}}^{(2)})}.\frac{s_{\text{w,air}}^{\text{BG}}(\Phi_{\text{g}}^{(2)})}{s_{\text{w,air}}^{\text{BG}}(\Phi_{\text{w}}^{(1)})}}{\frac{s_{\text{w,air}}^{\text{SA}}(\Phi_{\text{w}}^{(1)})}{s_{\text{w,air}}^{\text{BG}}(\Phi_{\text{w}}^{(1)})}}.\frac{p_{\text{g}}^{(2)}(z_{\text{g}}^{(2)})}{p_{\text{w}}^{(1)}(z_{\text{w-eq}})} \quad (5)$$

The following assumptions were made: (i) the ratio of W_{air} values between the two setups differed from unity by a negligible amount, (ii) the ratio of two ratios of Spencer-Attix and Bragg-Gray stopping-power ratios differed from unity by a negligible amount, (iii) the ratio of Bragg-Gray stopping-power ratios for different fluences differed from unity by a negligible amount and (iv) the ratio of perturbation factors between water and graphite differed from unity by a negligible amount. Based on these principles, fluence correction factors were calculated experimentally in a low-energy carbon-ion beam by a ratio of ionization curves in water ($M^{(1)}$) and graphite ($M^{(2)}$) [Rossomme *et al.*, 2013]:

$$k_{\text{fl,Rossomme}}^{\text{exp}} = \frac{M^{(1)}(z_{\text{w-eq}})}{M^{(2)}(z_{\text{g}}^{(2)})} \approx k_{\text{fl,dose}}^{\text{MC}} \quad (6)$$

The first assumption is supported by the fact that the spectra between setups at equivalent depths are marginally different and the short range of secondary electrons supports the second assumption. The third assumption is supported by the fact that the stopping-power ratios vary little with energy so for the two spectra, which are very similar, the stopping-power ratios are likely to be almost equal [Andreo *et al.*, 2000, Lühr *et al.*, 2011]. The fourth assumption cannot be satisfied since the ratio of perturbation correction factors between water and graphite ratio is not well known. The authors reported disagreements between fluence correction factors calculated numerically and experimentally which suggested that the ratio of ionization chamber perturbation correction factors between graphite and water is not negligible and it should be considered in equation (6).

2.2.3 *Depth-averaging approach.* In previous work [Lourenço *et al.*, 2016a], another approach was introduced to measure fluence correction factors experimentally between water and plastic materials in a high-energy carbon-ion beam. Here, the same formalism was applied to calculate fluence corrections between water and graphite. In this approach an alternative setup was used over setup #2. In this alternative setup, referred to as setup #3, measurements were performed in a water phantom after passing through graphite slabs of variable thicknesses (figure 1). Rewriting equation (4) using setups #1 and #3 gives:

$$\frac{M^{(1)}\left(z_{\mathrm{w}}^{(1)}\right)}{M^{(3)}\left(d^{(3)},t_{\mathrm{g}}\right)}=\frac{D_{\mathrm{w}}^{(1)}\left(z_{\mathrm{w}}^{(1)}\right)}{D_{\mathrm{w}}^{(3)}\left(d^{(3)},t_{\mathrm{g}}\right).\frac{W_{\mathrm{air}}^{(1)}/e}{W_{\mathrm{air}}^{(3)}/e}.\frac{s_{\mathrm{w,air}}^{\mathrm{SA}}(\Phi_{\mathrm{w}}^{(1)})}{s_{\mathrm{w,air}}^{\mathrm{SA}}(\Phi_{\mathrm{w}}^{(3)})}.\frac{p_{\mathrm{w}}^{(1)}\left(z_{\mathrm{w}}^{(1)}\right)}{p_{\mathrm{w}}^{(3)}\left(d^{(3)},t_{\mathrm{g}}\right)}} \quad (7)$$

where $d^{(3)}$ is the depth of measurement in setup #3 for a particular graphite thickness t_{g}. Depths in setups #1 and #3 are related by the difference of ranges. The assumptions were made that (i) the ratio of W_{air} values between setups #1 and #3 differed from unity by a negligible amount, (ii) the ratio of Spencer-Attix stopping-power ratios for $\Phi_{\mathrm{w}}^{(1)}$ and $\Phi_{\mathrm{w}}^{(3)}$ differed from unity by a negligible amount, (iii) the ratio of ionization chamber perturbation factors differed from unity by a negligible amount and (iv) when $d^{(3)}=0$ and $z_{\mathrm{g}}^{(2)}=t_{\mathrm{g}}$, the fluence in setup #3 equals the fluence in setup #2, $\Phi_{\mathrm{w}}^{(3)}(0,t_{\mathrm{g}})\approx\Phi_{\mathrm{g}}^{(2)}(t_{\mathrm{g}})$. Similar arguments to those described above support the first and second assumptions, and the fact that ionization chamber measurements are always performed in water supports the third assumption. Moreover, Verhaegen and Palmans (2001) showed that ionization chamber perturbation factors have only a slight variation with energy.

Based on assumption (iv), it was shown [Lourenço *et al.*, 2016a] that the ratio between dose in setup #3, $D_{\mathrm{w}}^{(3)}(0,t_{\mathrm{g}})$, and dose in setup #2, $D_{\mathrm{g}}^{(2)}(t_{\mathrm{g}})$, was approximately equal to the Bragg-Gray water-to-graphite stopping-power ratio, $s_{\mathrm{w,g}}^{\mathrm{BG}}(\Phi_{\mathrm{g}}^{(2)})$. Therefore, the fluence correction factor can be calculated by the ratio of ionization chamber readings in setups #1 and #3:

$$k_{\mathrm{fl,depth}}^{\mathrm{exp}}(t_{\mathrm{g,w-eq}})=\frac{M^{(1)}(z_{\mathrm{w}}^{(1)})}{M^{(3)}(0,t_{\mathrm{g}})}\approx\frac{D_{\mathrm{w}}^{(1)}\left(z_{\mathrm{w}}^{(1)}\right)}{D_{\mathrm{g}}^{(2)}(t_{\mathrm{g}}).s_{\mathrm{w,g}}^{\mathrm{BG}}(\Phi_{\mathrm{g}}^{(2)})}\approx k_{\mathrm{fl,dose}}^{\mathrm{MC}} \quad (8)$$

where $t_{\mathrm{g,w-eq}}$ is the water-equivalence thickness of the graphite slab t_{g}, derived from the difference of ranges between the setups #1 and #3. For a particular graphite slab t_{g} tested experimentally, the results indicated that the ratio $M^{(1)}(z_{\mathrm{w}}^{(1)})/M^{(3)}\left(d^{(3)},t_{\mathrm{g}}\right)$ varies little with the depth of measurement $d^{(3)}$, thus a mean value was derived:

$$k_{\mathrm{fl,depth}}^{\mathrm{exp}}(t_{\mathrm{g,w-eq}})\approx\frac{1}{N}\sum_{j=1}^{N}\frac{M^{(1)}(z_{\mathrm{w}}^{(1)})}{M^{(3)}\left(d_j^{(3)},t_{\mathrm{g}}\right)} \quad (9)$$

Here, this approach is referred to as the depth-averaging method and it was used to determine k_{fl} factors experimentally. Note that values near the Bragg peak were not considered since the effect of positioning errors is critical in that region due to high dose gradients. By testing graphite slabs of variable thicknesses t_{g}, the variation of the fluence correction factor with depth was studied.

The depth-averaging approach was also applied to the results of Monte Carlo simulations of setups #1 and #3:

$$k_{\mathrm{fl,depth}}^{\mathrm{MC}}(t_{\mathrm{g,w-eq}})\approx\frac{1}{N}\sum_{j=1}^{N}\frac{D_{\mathrm{w}}^{(1)}(z_{\mathrm{w}}^{(1)})}{D_{\mathrm{w}}^{(3)}\left(d_j^{(3)},t_{\mathrm{g}}\right)} \quad (10)$$

In a previous study [Lourenço *et al.*, 2016b], fluence correction factors between water and graphite were calculated in proton beams using similar methods. For proton beams, fluence corrections derived from setups #1 and #3 were found to be partial fluence corrections since they account only for primary and part of the secondary particles spectra. In these beams, secondary particles, such as alpha particles, which originated from target fragmentation with very short ranges, do not have sufficient energy to cross the chamber's wall.

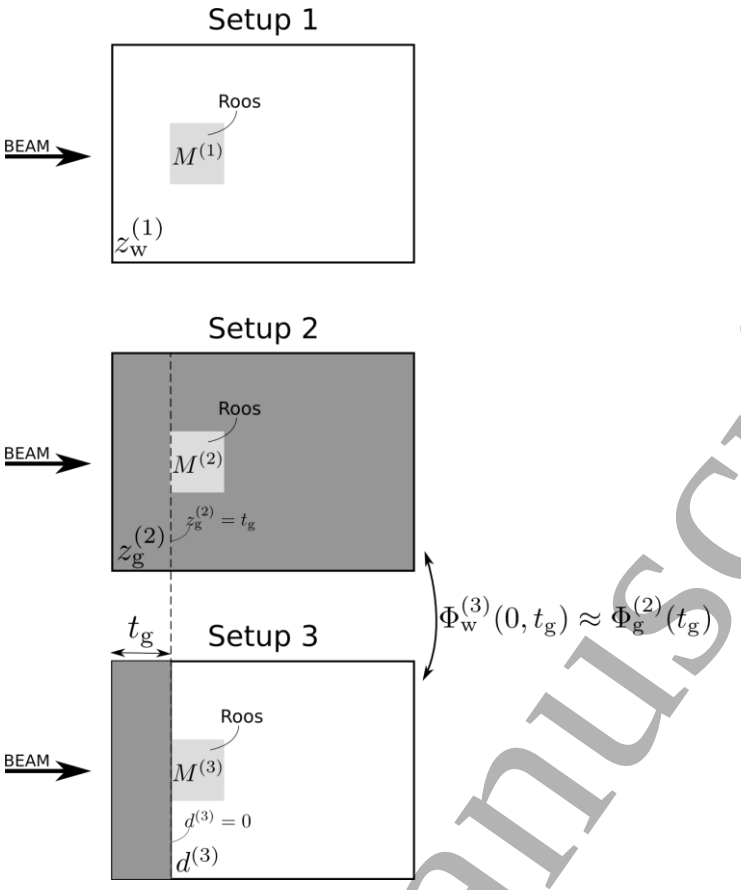

Figure 1. Schematic representation of setups #1, #2 and #3. The white colour in setup #1 and #3 represents a phantom of water. In setup #2 the grey colour represents a phantom of graphite and in setup #3, it represents graphite slabs of variable thickness t_{g}. Adapted from Lourenço *et al.* (2016a and 2016b).

3. Methods

3.1. Experimental fluence correction factor, $k_{\mathrm{fl,depth}}^{\mathrm{exp}}$

Measurements were performed at the Gunma University Heavy Ion Medical Center (GHMC), Japan [Komori *et al.*, 2004, Yonai *et al.*, 2008, Ohno *et al.*, 2011], using a carbon-ion beam with mean energy of 290 MeV/n at the source. Measurements were performed with a field size of 11 x 11 cm², without modulation. Fluence corrections were measured using a plane-parallel Roos ionization chamber (PTW type 34001, radius of the collecting volume = 0.75 cm) due to its small collecting volume in comparison with the field size. Central axis measurements should be performed in broad beams using small detectors, while laterally integrated measurements should be performed in pencil beams using larger detectors. Reference dosimetry in scanned beams is usually performed using pencil beams, thus, these corrections could be generalized to scanned beams as well. For monitoring purposes a cylindrical Farmer ionization chamber (PTW type 30011) was placed in the corner of the collimator exit. Measurements were performed with a constant source-to-detector distance (SDD), so no correction was required for the inverse square law. Experimental information on fluence correction factors was obtained from ionization chamber measurements in water (figure 1). This procedure was repeated for graphite plates (t_{g}) with 0.09, 1.9, 5.5, 7.4 and 9.2 g.cm^{-2} thicknesses placed in front of the water phantom. Ionization chamber readings were corrected for temperature and pressure. Ion recombination and polarity corrections were not considered since the same ionization chamber was used in the two setups and a ratio of two ionization chamber readings was calculated. Moreover, the two measurement points have almost identical dose rates and particle spectra.

The standard uncertainty on each value of $k_{\mathrm{fl,depth}}^{\mathrm{exp}}$ was estimated to be 0.24% ($k = 1$) and the sources of uncertainties are listed in table 1. Type A uncertainties included repeatability and type B uncertainties included uncertainties in temperature and pressure measurements and the standard deviation of the mean value $k_{\mathrm{fl,depth}}^{\mathrm{exp}}$ (equation (9)), which is referred as $s_{\left[k_{\mathrm{fl,depth}}^{\mathrm{exp}}\right]}$. The $k_{\mathrm{fl,depth}}^{\mathrm{exp}}$ factor is calculated from a ratio of ionization chamber

readings from setups #1 and #3 and since the same type of electrometer was used, uncertainties related to the electrometer were correlated and cancel out. The same applies to ion recombination uncertainties since the same ionization chamber was used in the two setups considered. Uncertainties related to the assumptions that W_{air}, $s_{\mathrm{w,air}}^{\mathrm{SA}}$ and p_{w} are the same for setups #1 and #3, as well as, an uncertainty contribution for positioning reproducibility were considered negligible.

Standard uncertainties (%)	**Type A**	**Type B**
Repeatability: Roos/Monitor	0.17	-
Temperature	-	0.05
Pressure	-	0.05
$s_{\left[k_{\mathrm{fl,depth}}^{\mathrm{exp}}\right]}$	-	0.15
Overall	**0.17**	**0.17**
Combined	**0.24**	

Table 1. Contributions to the experimental uncertainty of $k_{\mathrm{fl,depth}}^{\mathrm{exp}}$.

3.2. Numerical fluence correction factor, $k_{\mathrm{fl,fluence}}^{\mathrm{MC}}$, $k_{\mathrm{fl,dose}}^{\mathrm{MC}}$ and $k_{\mathrm{fl,depth}}^{\mathrm{MC}}$

Fluence corrections were also obtained with Monte Carlo simulations through the implementation of three methods based on (i) the fluence distributions differential in energy, thus defining $k_{\mathrm{fl,fluence}}^{\mathrm{MC}}$ (refer to equation (1)), (ii) a ratio of calculated doses in water and graphite at equivalent depths, thus defining $k_{\mathrm{fl,dose}}^{\mathrm{MC}}$ (refer to equation (2)), and (iii) simulations of the experimental setup, thus defining $k_{\mathrm{fl,depth}}^{\mathrm{MC}}$ (refer to equation (10)).

Simulations were performed with FLUKA version 2011.2c.3 [Ferrari *et al.*, 2005, Böhlen *et al.*, 2014], using the default card HADRONTHErapy and delta-ray production set to infinite threshold. For the calculation of $k_{\mathrm{fl,dose}}^{\mathrm{MC}}$ and $k_{\mathrm{fl,fluence}}^{\mathrm{MC}}$, depth-dose distributions and fluence spectra differential in energy were scored in homogenous phantoms of water (setup 1) and graphite (setup 2). For the calculation of $k_{\mathrm{fl,depth}}^{\mathrm{MC}}$, setup 3 was also simulated in FLUKA. Dose and fluence were scored in bins of 0.007 cm and 0.1 cm, respectively, throughout the phantoms. The beam energy and spread were tuned against experimental data for 265 MeV/n and σ=0.75 MeV, respectively, at the phantom surface. Note that the beam energy is 290 MeV/n at the source, which corresponds to the energy of the beam before the exit window of the vacuum chamber. The presence of a scatterer and air in the beam line reduces the residual range in the water phantom [Ohno *et al.*, 2011]. A broad carbon-ion beam of 11 x 11 cm^2 without modulation was simulated, with the radius of the scoring region equal to the radius of the Roos chamber used in the experiments. In addition, a beam without divergence was considered since the measurements were performed at constant SDD. A total number of 25x10^6 carbon-ion histories was required for each setup to obtain a standard uncertainty (type A) below 0.3%. Type B Monte Carlo uncertainties include stopping powers and interaction cross-sections uncertainties and were not considered [Lourenço *et al.*, 2016a]. The ICRU Report 73 (2005) compared stopping powers from different models with experimental data and values agreed within 10%. In the calculation of the fluence correction factor using Monte Carlo methods (equations (1) and (2)), the stopping powers are used in a ratio and thus uncertainties related with stopping powers will be strongly correlated. With regards to interaction cross-sections uncertainty, Böhlen *et al.* (2010) compared nuclear models from FLUKA with experimental data for carbon-ion beams interacting with water and polycarbonate, which contains carbon. The results showed that for integral fragment yields FLUKA could predict experimental data within uncertainties, although for non-differential quantities disagreements of the order of tens of percent were reported. Palmans *et al.* (2013) estimated fluence correction factors between water and graphite in a low-energy monoenergetic proton beam from an analytical model and simulations using five different Monte Carlo codes. For the analytical model, nuclear data from ICRU Report 63 (2000) was used where uncertainties of the order of 5%-10% for total non-elastic nuclear interactions and 20%-30% on the angle-integrated production cross sections for secondary particles are reported. In the work by Palmans *et al.* (2013), maximum differences of k_{fl} factors from different models were of 1%. Therefore, although the large uncertainties in the nuclear data (ICRU, 2000), its influence in the calculation of k_{fl} factors is small.

4. Results and discussion

4.1. Monte Carlo simulations: $k_{\mathrm{fl,fluence}}^{\mathrm{MC}}$ *and* $k_{\mathrm{fl,dose}}^{\mathrm{MC}}$

In figure 2, the contributions of primary and secondary particles to the absorbed dose calculated with FLUKA are shown for a 265 MeV/n carbon-ion beam in water (solid lines) and graphite (dashed lines). Primary carbon ions that undergo an elastic nuclear interaction are considered as primaries and all products from a non-elastic nuclear interaction are considered secondary, including charge-changing products. Primary carbon ions do not contribute to the dose tail behind the Bragg peak. In carbon-ion beams, projectile fragments emerging with similar velocity to the projectile but with larger ranges dominate the secondary particle spectrum. Results are in agreement with experimental data from Haettner *et al.* (2013) and with previous Monte Carlo studies from Kempe *et al.* (2007) and Rossomme *et al.* (2013), using SHIELD-HIT and Geant4/GATE codes, respectively. The benchmark of our simulations was discussed in detail in Lourenço *et al.* (2016a).

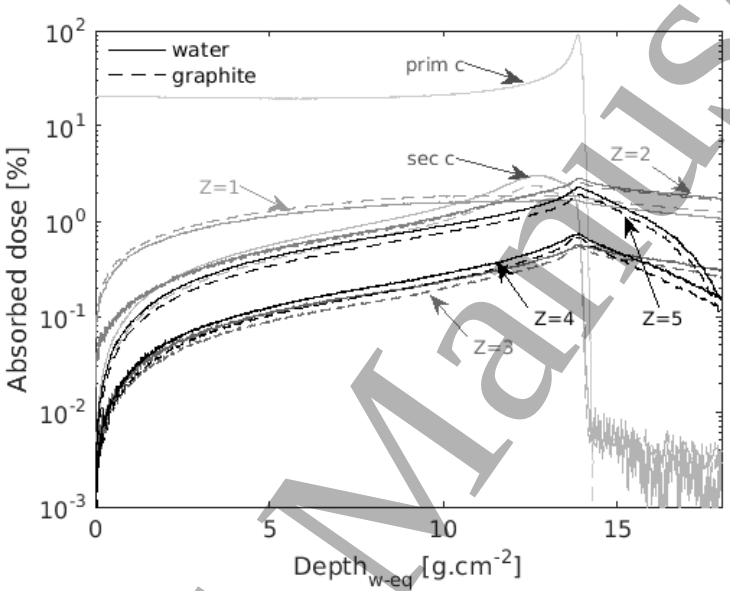

Figure 2. Depth-dose distributions for a 265 MeV/n carbon-ion beam in a water (solid lines) and graphite (dashed lines) phantoms for different particles (prim c = primary carbon ions, sec c = secondary carbon ions, and particles with atomic numbers Z=1, Z=2, Z=3, Z=4 and Z=5). Curves were normalised to the maximum of the total dose and are presented on a logarithmic scale.

Figure 3 shows the calculated fluence correction factor between water and graphite as a function of depth for different sets of particles. A good agreement was found between the fluence, $k_{\mathrm{fl,fluence}}^{\mathrm{MC}}$, and dose, $k_{\mathrm{fl,dose}}^{\mathrm{MC}}$, methods (0.05% difference). At the surface, the primary carbon-ion fluence is the same in both phantoms. When all particles are considered, there is a slight reduction of the k_{fl} term (0.998) due to the very short range of secondary particles from target fragmentation. Compared to proton beams [Palmans *et al.*, 2013], the reduction of the k_{fl} term at the surface is less pronounced for carbon-ion beams because the secondary particle spectrum is much more dominated by projectile fragmentation and thus secondary particles emerge with larger ranges.

When considering only primary carbon ions, k_{fl} decreases slightly in depth (toward 0.99) because more primary particles are removed from the beam in water than in graphite. When also secondary carbon ions are included, k_{fl} increases towards 1.02 at a depth near the Bragg peak since the total charge-changing cross-sections are higher in water than in graphite [Hultqvist *et al.*, 2012]. Therefore, the dose contribution of secondary carbon ions is also higher in water than in graphite as shown in figure 2. The same applies when a different set of charged particles are included, with exception of fragments with Z=1 of which the dose contribution is higher in graphite than in water (figure 2), thus there is a reduction in the k_{fl} factor when these particles are included.

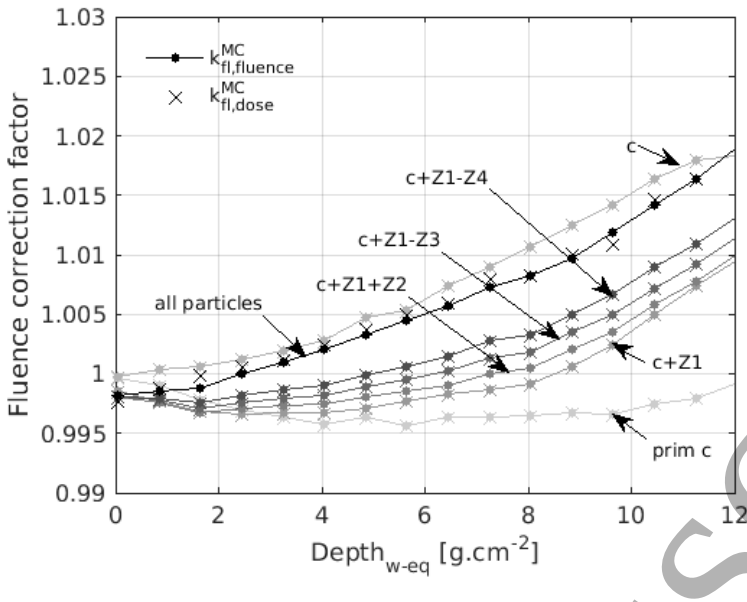

Figure 3. Fluence correction factor between water and graphite derived for different set of particles (prim c = primary carbon ions, c = primary and secondary carbon ions, and particles with atomic numbers Z=1 (Z1), Z=2 (Z2), Z=3 (Z3), Z=4 (Z4) and Z=5 (Z5)). Circles represent the fluence-based method and crosses represent the dose-based method.

4.2. Comparison between Monte Carlo simulations and experimental data

A comparison between experimental data and numerical simulations of the fluence correction factor is presented in figure 4. The results from different calculation methods are presented in this figure: the fluence- and depth-averaging approaches derived from Monte Carlo simulations and the depth-averaging approach derived from experimental data. For all methods, the fluence correction factor increased with depth from 1.00 to 1.02. The average difference between experimental and numerical simulations was of the order of 0.11% for the depth-averaging method and 0.16% for the fluence method. These results suggest that k_{fl} obtained experimentally includes all charged particles contrary to the case of protons [Lourenço *et al.*, 2016b]. Similar results were found by Rossomme *et al.* (2013) for a clinical 80 MeV/n carbon-ion beam using Geant4 and experimental data. In their work, fluence corrections were obtained using setups #1 and #2, assuming that the ratio of perturbations factors between water and graphite was negligible. However, small inconsistencies between numerical and experimental data were reported, which suggested that perturbation factors should be included in the analysis. In this work, by always measuring ionization chamber readings in water, using setups #1 and #3, it can be assumed that perturbation factors are the same for both setups. Our results are also in agreement with the results from Lühr *et al.* (2011). In their work, a Monte Carlo study was performed, using the SHIELD-HIT10A code, to determine fluence corrections for graphite in comparison to water in 107 MeV/n, 270 MeV/n and 400 MeV/n carbon-ion beams. For the 107 MeV/n and 270 MeV/n carbon-ion beams, corrections deviated from unity by 0% at the surface to 1% at a depth near the Bragg peak, while for the 400 MeV/n carbon-ion beam corrections deviated from unity by 0% at the surface to 2% at a depth near the Bragg peak. As expected, the fluence correction factor near the Bragg peak is greater for higher incident energies than for lower incident energies, due to the extra nuclear interactions that occur as the carbon-ion beam slows down.

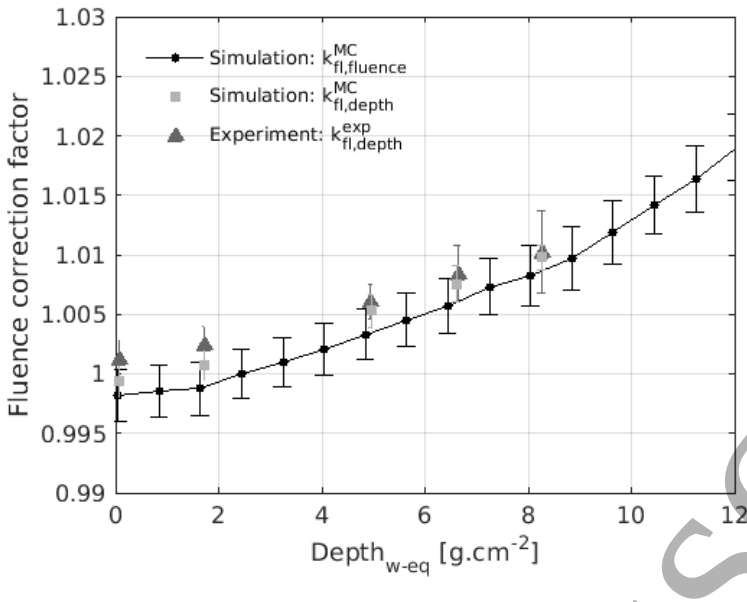

Figure 4. Fluence correction factor between water and graphite derived using different methods. Circles represent the fluence-based method (all particles), $k^{MC}_{fl,fluence}$, squares and triangles represent the depth-averaging method obtained from simulations, $k^{MC}_{fl,depth}$, and experiments, $k^{exp}_{fl,depth}$, respectively.

5. Conclusions

In this work, a formalism was developed and adapted to derive absorbed dose to water, using a graphite calorimeter in carbon-ion beams. This procedure has the advantage of involving measurements being done independently from ionization chamber perturbation factors caused by the use of different phantom materials. Fluence corrections, needed for the conversion of dose to graphite from a graphite calorimeter to dose to water, were measured experimentally in a high-energy carbon-ion beam and compared with numerical simulations.

The results showed that k_{fl} obtained from experiments includes all charged particles contrary to the case of protons. For graphite, the fluence correction factor increased in depth from 1.00 towards 1.02 and the average difference between experimental and numerical simulations was of the order of 0.13%. The magnitude of differences between methods supports the use of FLUKA to compute fluence correction factors for carbon-ion beams between water and graphite. The work presented here will feed into the establishment of graphite calorimetry in carbon-ion beams by using a more practical experimental setup for the conversion of dose to graphite to dose to water.

Acknowledgements

The authors would like to thank Simon Duane for useful discussions. The authors acknowledge the use of the UCL Legion High Performance Computing Facility (Legion@UCL), and associated support services, in the completion of this work, and the FLUKA mailing list for all the support with FLUKA code. A.L. was supported by University College London and the UK National Physical Laboratory through the National Measurement System.

References

Andreo P, Burns D T, Hohlfeld K, Huq M S, Kanai T, Laitano F, Smyth V G and Vynckier S 2000 Absorbed dose determination in external beam radiotherapy: an international code of practice for dosimetry based on standards of absorbed dose to water IAEA *Technical Report Series 398* (Vienna: IAEA)

AAPM, Protocol for heavy charged-particle therapy beam dosimetry; a report of Task Group 20 1986 Radiation Therapy Committee, American Association of Physicists in Medicine Report 16, American Institute of Physics

Böhlen T T, Cerutti F, Dosanjh M, Ferrari A, Gudowska I, Mairani A and Quesada J M 2010 Benchmarking nuclear models of FLUKA and GEANT4 for carbon ion therapy *Phys. Med. Biol.* **55** 5833–47

Böhlen T T, Cerutti F, Chin M P W, Fassò A, Ferrari A, Ortega P G, Mairani A, Sala P R, Smirnov G and Vlachoudis V 2014 The FLUKA Code: Developments and Challenges for High Energy and Medical Applications *Nuclear Data Sheets* **120** 211-214

Brede H J, Greif K D, Hecker O, Heeg P, Heese J, Jones D T, Kluge H and Schardt D 2006 Absorbed dose to water determination with ionization chamber dosimetry and calorimetry in restricted neutron, photon, proton and heavy-ion radiation fields *Phys. Med. Biol.* **51** 3667–82

Ding G X, Rogers D W O, Cygler J E and Mackie T R 1997 Electron fluence correction factors for conversion of dose in plastic to dose in water *Med. Phys.* **24** 161-76

Ferrari A, Sala P R, Fassò A and Ranft J 2005 FLUKA: a multi-particle transport code *CERN-2005-10, INFN/TC_05/11, SLAC-R-773*

Haettner E, Iwase H, Krämer M, Kraft G and Schardt D 2013 Experimental study of nuclear fragmentation of 200 and 400 MeV/u (12)C ions in water for applications in particle therapy *Phys. Med. Biol.* **58** 8265-79

Hultqvist M, Lazzeroni M, Botvina A, Gudowska I, Sobolevsky N and Brahme A 2012 Evaluation of nuclear reaction cross-sections and fragment yields in carbon beams using the SHIELD-HIT Monte Carlo code. Comparison with experiments *Phys. Med. Biol.* **57** 4369–85

ICRU 1998 Clinical Proton Dosimetry Part I: Beam Production, Beam Delivery and Measurement of Absorbed Dose ICRU Report 59 (Bethesda MD: ICRU)

ICRU 2000 Nuclear Data for Neutron and Proton Radiotherapy and for Radiation Protection ICRU Report 63 (Bethesda MD: ICRU)

ICRU 2005 Stopping of Ions Heavier Than Helium ICRU Report 73 (Bethesda MD: ICRU)

Kempe J, Gudowska I and Brahme A 2007 Depth absorbed dose and LET distributions of therapeutic 1H, 4He, 7Li, and 12C beams *Med. Phys.* **34** 183-92

Komori M, Furukawa T and Kanai T 2004 Optimization of spiral-wobbler system for heavy-ion radiotherapy *Jpn. J. Appl. Phys.* **43** 6463–6467

Lourenço A, Wellock N, Thomas R, Homer M, Bouchard H, Kanai T, MacDougall N, Royle G, Palmans H 2016 Theoretical and experimental characterization of novel water-equivalent plastics in clinical high-energy carbon-ion beams *Phys. Med. Biol.* **61** 7623-38

Lourenço A, Thomas R, Bouchard H, Kacperek A, Vondracek V, Royle G, Palmans H 2016 Experimental and Monte Carlo studies of fluence corrections for graphite calorimetry in low- and high-energy clinical proton beams *Med. Phys.* **43** 4122-32

Lühr A, Hansen D, Sobolevsky N, Palmans H, Rossomme S and Bassler N 2011 Fluence correction factors and stopping power ratios for clinical ion beams *Acta Oncol.* **50** 797–805

Medin J 2010 Implementation of water calorimetry in a 180 MeV scanned pulsed proton beam including an experimental determination of kQ for a Farmer chamber *Phys. Med. Biol.* **55** 3287–98

Paganetti H 2009 Dose to water versus dose to medium in proton beam therapy *Phys. Med. Biol.* **54** 4399-421

Palmans H, Symons J E, Denis J-M, de Kock E A, Jones D T L and Vynckier S 2002 Fluence correction factors in plastic phantoms for clinical proton beams *Phys. Med. Biol.* **47** 3055–71

Palmans H, Thomas R, Simon M, Duane S, Kacperek A, DuSautoy A and Verhaegen F 2004 A small-body portable graphite calorimeter for dosimetry in low-energy clinical proton beams *Phys. Med. Biol.* **49** 3737–3749

Palmans H, Bailey M, Duane S, Shipley D and Thomas R 2007 Development of a primary standard level proton calorimeter at NPL *Radiother. Oncol.* **84** (Suppl. 1) S135

Palmans H, Al-Sulaiti L, Andreo P, Shipley D, Lühr A, Bassler N, J Martinkovič, Dobrovodský J, Rossomme S, Thomas R and Kacperek A 2013 Fluence correction factors for graphite calorimetry in a low-energy clinical proton beam. I. Analytical and Monte Carlo simulations *Phys. Med. Biol.* **58** 3481–3499

Ohno T, Kanai T, Yamad S, Yusa K, Tashiro M, Shimada H, Torikai K, Yoshida Y, Kitada Y, Katoh H, Ishii T and Nakano T 2011 Carbon ion radiotherapy at the Gunma University Heavy Ion Medical Center: New Facility Setup *Cancers* **3** 4046-60

Rossomme R, Palmans H, Shipley D, Thomas R, Lee N, Romano F, Cirrone P, Cuttone G, Bertrand D and Vynckier 2013 Conversion from dose-to-graphite to dose-to-water in an 80 MeV/A carbon ion beam *Phys. Med. Biol.* **58** 5363–5380

Sakama M, Kanai T, Fukumura A and Abe K 2009 Evaluation of w values for carbon beams in air, using a graphite calorimeter *Phys. Med. Biol.* **54** 1111–30

Sarfehnia A, Clasie B, Chung E, Lu H M, Flanz J, Cascio E, Engelsman M, Paganetti H and Seuntjens J 2010 Direct absorbed dose to water determination based on water calorimetry in scanning proton beam delivery *Med. Phys.* **37** 3541–50

Schneider U, Pemler P, Besserer J, Dellert M, Moosburger M, de Boer J, Pedroni E and Boehringer T 2002 The water equivalence of solid materials used for dosimetry with small proton beams *Med. Phys.* **29** 2946-51

1 Seuntjens J, Olivares M, Evans M, Podgorsak E 2005 Absorbed dose to water reference dosimetry using solid phantoms in the context of absorbed-dose protocols *Med. Phys.* **32** 2945-53
2 Verhaegen F and Palmans H 2001 A systematic Monte Carlo study of secondary electron fluence perturbation in clinical proton beams (70–250 MeV) for cylindrical and spherical ion chambers," *Med. Phys.* **28** 2088–2095
3 Vynckier S, Bonnett D and Jones D 1991 Code of practice for clinical proton dosimetry *Radiother. Oncol.* **20** 53–63
4 Vynckier S, Bonnett D and Jones D 1994 Supplement to the code of practice for clinical proton dosimetry *Radiother. Oncol.* **32** 174–179
5 Yonai S, Kanematsu N, Komori M, Kanai T, Takei Y, Takahashi O, Isobe Y, Tashiro M, Koikegami Hand Tomita 2008 H Evaluation of beam wobbling methods for heavy-ion radiotherapy *Med. Phys.* **35** 927–938